CrossMark

Heart valve scaffold fabrication: Bioinspired control of macro-scale morphology, mechanics and micro-structure

Antonio D'Amore [a, b, c, d, e], Samuel K. Luketich [c, f], Giuseppe M. Raffa [g], Salim Olia [a, c, h], Giorgio Menallo [a, c], Antonino Mazzola [a, e], Flavio D'Accardi [a, e], Tamir Grunberg [a, i], Xinzhu Gu [b, c], Michele Pilato [g], Marina V. Kameneva [a, b, c], Vinay Badhwar [c, j], William R. Wagner [a, b, c, f, *]

[a] Department of Bioengineering, University of Pittsburgh, Pittsburgh, PA, USA
[b] Department of Surgery, University of Pittsburgh, Pittsburgh, PA, USA
[c] McGowan Institute for Regenerative Medicine, University of Pittsburgh, Pittsburgh, PA, USA
[d] Fondazione RiMED, Italy
[e] Dipartimento innovazione industriale e digitale (DIIT), Università di Palermo, Italy
[f] Department of Chemical Engineering, University of Pittsburgh, Pittsburgh, PA, USA
[g] Istituto mediterraneo trapianti e terapie ad alta specializzazione (ISMETT), UPMC, Italy
[h] Artificial Heart Program, University of Pittsburgh Medical Center, Pittsburgh, PA, USA
[i] ORT Braude College of Engineering, Israel
[j] Dep. of Cardiovascular and Thoracic Surgery, West Virginia University, Morgantown, WV, USA

ARTICLE INFO

ABSTRACT

Valvular heart disease is currently treated with mechanical valves, which benefit from longevity, but are burdened by chronic anticoagulation therapy, or with bioprosthetic valves, which have reduced thromboembolic risk, but limited durability. Tissue engineered heart valves have been proposed to resolve these issues by implanting a scaffold that is replaced by endogenous growth, leaving autologous, functional leaflets that would putatively eliminate the need for anticoagulation and avoid calcification. Despite the diversity in fabrication strategies and encouraging results in large animal models, control over engineered valve structure-function remains at best partial. This study aimed to overcome these limitations by introducing double component deposition (DCD), an electrodeposition technique that employs multi-phase electrodes to dictate valve macro and microstructure and resultant function. Results in this report demonstrate the capacity of the DCD method to simultaneously control scaffold macro-scale morphology, mechanics and microstructure while producing fully assembled stent-less multi-leaflet valves composed of microscopic fibers. DCD engineered valve characterization included: leaflet thickness, biaxial properties, bending properties, and quantitative structural analysis of multi-photon and scanning electron micrographs. Quasi-static *ex-vivo* valve coaptation testing and dynamic organ level functional assessment in a pressure pulse duplicating device demonstrated appropriate acute valve functionality.

© 2017 Published by Elsevier Ltd.

1. Introduction

Heart valve disease represents a major cause of morbidity and mortality, with age and sex adjusted prevalence for the US population reported as 2.5% [1], with mitral and aortic regurgitation or stenosis being frequent syndromes. While the incidence of different etiologies varies based on age and geography [2], the major mechanisms initiating valvular maladies remain degenerative, rheumatic or inflammatory processes, ischemic cardiomyopathy and congenital malformations [3]. Globally, the valve replacement and repair market was estimated as $2.8 B with an expected compound annual growth rate of 9.1% [4].

* Corresponding author. McGowan Institute for Regenerative Medicine, Professor of Surgery, Bioengineering and Chemical Engineering, University of Pittsburgh, Bridgeside Point Building II, 450 Technology Drive, Suite 300, Pittsburgh, PA 15219, USA.
E-mail address: wagnerwr@upmc.edu (W.R. Wagner).

Two classes of heart valve prostheses respond to these clinical and market needs: mechanical and bioprosthetic. Mechanical valves benefit from longevity, but come with the burden of chronic anticoagulation therapy due to an elevated risk for thrombosis and thromboembolism [5]. Conversely, bioprosthetic valves do not require chronic anticoagulation therapy. However, their long term performance and durability remains plagued by failure modalities that include leaflet tear and calcific degeneration, with the latter risk elevated in younger patients [6]. Tissue engineered heart valves (TEHVs) have been proposed to resolve these issues by implanting a scaffold that is replaced or extensively augmented with endogenous tissue growth, leaving autologous, functional leaflets that would putatively eliminate the need for anticoagulation therapy and avoid tissue calcification. While this approach has never been fully demonstrated *in vivo* [7—9], a wide variety of efforts have been directed to overcome the substantial challenges associated with translating TEHV technology toward clinical practice. Multidisciplinary strategies have been explored in terms of cell source [10—12], engineered construct conditioning regimens [13,14], and transcatheter deployment strategies [15,16]. Processing technologies developed include non-woven meshes molded by heat welding [17], salt leaching [11], stereolithography [18], polymer dipping [19,20], fiber-reinforced composite molding [21], electrospinning [22], jet spraying [23] and acid etching of Nitinol sheets [24,25]. In developments based on natural materials, of promise are decellularized tissue sheets [26] and whole organ decellularization protocols for allografts [27,28] or xenografts [29,30] as well as collagen cross-linking strategies for pericardial tissue [31] and *in vivo* [32] or in vitro [14,33] conditioning that facilitates the structured growth of neo-tissue.

Despite the diversity in fabrication strategies reported and some of the encouraging results in large animal models, control over engineered construct structure-function remains at best partial. More specifically, the current technologies do not allow for the combined engineering of four major design factors: I) macroscopic morphology and size (e.g. aortic, mitral, tricuspid, pulmonary indications), II) in-plane mechanics (e.g. biaxial response), III) out of plane mechanics (e.g. bending rigidity), and IV) microstructure (e.g. fiber diameter, pore size). This study aims to overcome these limitations by introducing an electrodeposition technique that employs multi-phase electrodes to control valve macro and microstructure and resultant function.

The double component deposition (DCD) technique reported here utilizes electrodes composed of electrically conducting/insulating materials to selectively orient fiber deposition on anatomy inspired valve geometries (Figs. 1—3). The first component, made of electrically conducting metallic alloy, acts as an electrospun polymer collection surface, while the second component, made of materials with lower conductivity, reduces fiber deposition in regions which would otherwise receive excessive mass accumulation during the fabrication process. Results in this report demonstrate the capacity of the DCD method to simultaneously control scaffold macro-scale morphology, mechanics, and microstructure while producing stent-less multi-leaflet valves composed of microscopic fibers. DCD engineered valve characterization included: leaflet thickness, biaxial properties, bending properties, multi-photon and scanning electron microscopy quantitative structural analysis, quasi-static *ex-vivo* valve coaptation testing and dynamic organ level functional assessment in a pressure pulse duplicator apparatus.

2. Methods

2.1. Mandrel design for double component fibers deposition (DCD)

The DCD mandrel model was developed in Solidworks (Waltham, MA, USA) and consisted of two components. The heart valve shaped conductive component was obtained by machining of aluminum alloy whereas the non-conductive component was made of acrylonitrile butadiene styrene (ABS) processed by injection molding (Fig. 1a,g). The heart valve shaped collecting surface was connected with a high voltage generator, and the "shield" component was mechanically connected to the motor providing the rotation. A second motor controlled the translational rastering speed [34,35]. The conductive component diameter was selected to be 40 mm based on echocardiography data by Ring et al. [36] of the anterior-posterior diameter D and septal-lateral diameter of human tricuspid valves throughout the cardiac cycle. The height h was calculated based on the diameter utilizing a h/D ratio of 1.6 utilized in the Sapien 3 prosthesis (Carpentier-Edwards, Irvine, CA). Leaflet profile was modeled as described with detail in Ref. [37], a design method that minimizes the central opening of the valve, targeting a central open area <1% of the orifice area (Figs. 1a,g and 2).

2.2. Double component fiber deposition (DCD) processing conditions

Poly(ester urethane) urea (PEUU) was synthesized as described in Ref. [38], and biodegradable valves were fabricated with electrospinning [39] using the developed mandrel for DCD and the following process variables: polymer voltage 11 kV, mandrel voltage −5 kV, polymer gap 15.5 cm, polymer flow rate 1.5 mL/h, polymer 12% w/v in HFIP, mandrel tangential velocities 0.3—3 m/s, mandrel rastering velocities 0—2.5 cm/s (Figs. 1—7, and 10 and Supplemental video 1—3). DCD capacity to tune microstructure and duplicate native leaflet fiber bundles diameter or pore size (Fig. 8f and g) was assessed by comparing leaflets fabricated under different conditions (polymer - mandrel voltage difference: 4—32 kV, gap: 5.5—7.5 cm, polymer/solvent concentration: 4—12%) with decellularized porcine valve leaflet tissue (Fig. 9).

Supplementary video related to this article can be found at https://doi.org/10.1016/j.biomaterials.2017.10.011.

2.3. Engineered leaflet thickness measurements

In order to assess the capacity of DCD to reproduce native valve leaflet thickness for the four valve types, the relationship between leaflet thickness and processing time was characterized. Native and electrospun leaflets (n ≥ 3/group) were dissected from the whole valve, and thickness measurements were taken with a dial indicator gage (Starrett, Athol, MA) on five locations spanning from the free edge to the belly and the commissural regions. The experimental error due to the valve leaflet wet content was minimized by performing each measurement 5 min after the leaflet was positioned on the gage [40,41]. The mean thickness values of the electrospun valves were plotted against the polymer deposition time for four independent fabrication times and then compared with the native tricuspid porcine valve. Based on the linear interpolation of these experimental points, the deposition time required to generate leaflets with native tricuspid porcine valve thickness was identified and tricuspid engineered valves with tailored leaflets thickness were fabricated (Fig. 1f). Engineered valve leaflets fabricated with these conditions were further tested (n=4) to assess the capacity of the design paradigm to be used in controlling the average leaflet thickness. Last, in order to further characterize the quality of the DCD in terms of surface homogeneity, maps for engineered and native valves were obtained by biquintic numerical interpolation (Matlab, MathWorks, Natick, MA) of thicknesses experimentally measured at fifteen different leaflet locations described above and on equally distributed locations around the leaflets edges (Figs. 1h—i and 3).
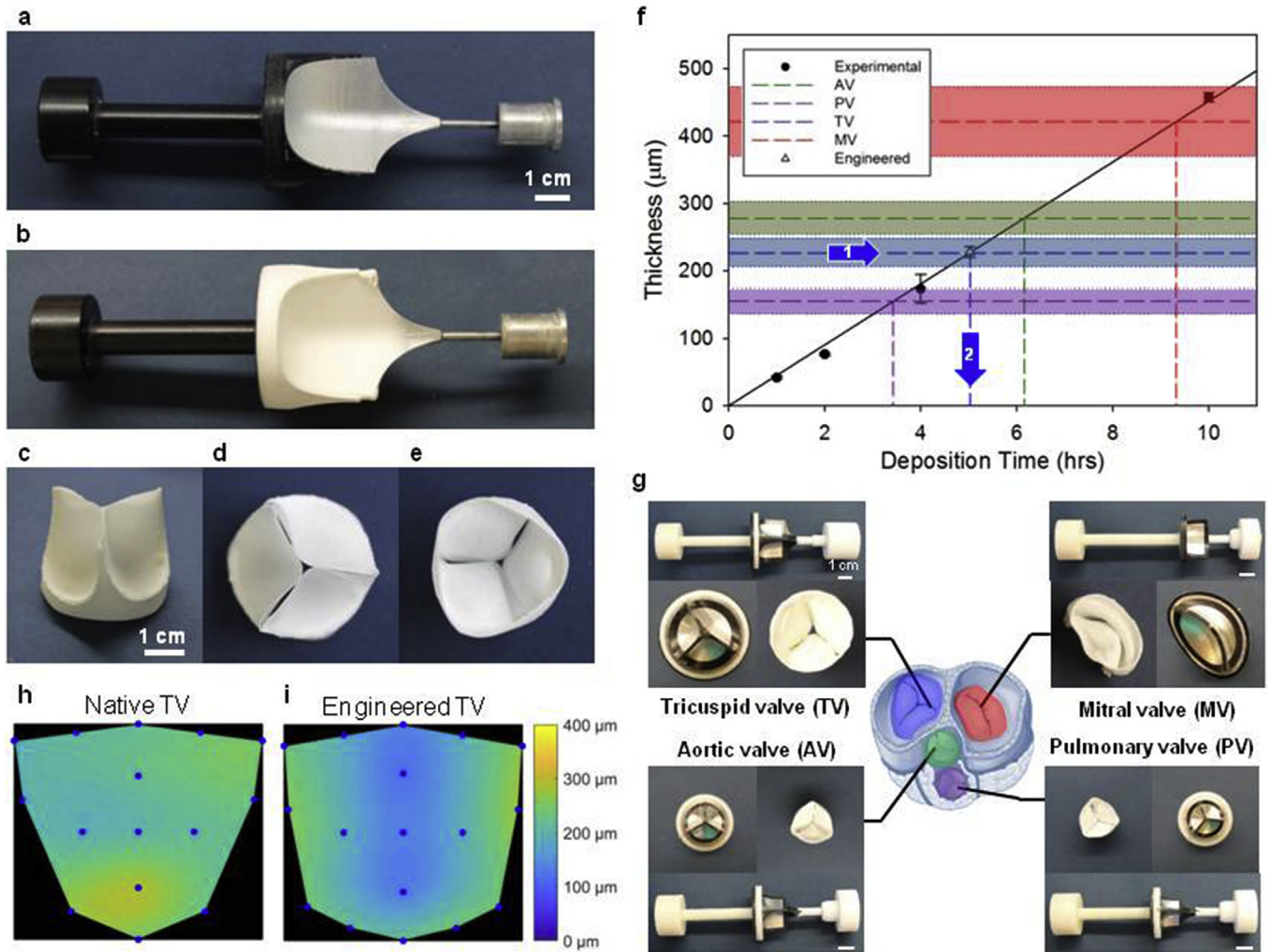
Fig. 1. Double component fiber deposition (DCD) process control of engineered heart valve morphology. a) Double component mandrel full assembly before fiber deposition. Mandrel component 1: non-conductive shield of acrylonitrile butadiene styrene (in black). Component 2: main collecting target of aluminum alloy. **b)** Double component mandrel after polymer fiber deposition (Supplemental Video 1). **c)** Tri-leaflet valve removed from the mandrel and trimmed, showing leaflet coaptation at rest. **d)** View from the ventricular side and **e)** view from the atrial side of the tri-leaflet valve. **f)** Process scalability in terms of construct thickness was verified by monitoring the leaflet thickness vs. deposition time. A specific thickness of interest was then fabricated to approximate a native porcine tricuspid valve (average thickness 227 µm) from a prescribed fabrication time of 5 h and 2 min to obtain comparable thickness in the artificial leaflets. Leaflet fabrication was evaluated in a range of interest for tissue engineering applications: 0–500 µm. Different colors illustrate thickness ranges for porcine valves and fabrication times for the four valve types. **g)** DCD processing method applied to the four valve types, prototypes shown in the picture demonstrate the capacity of DCD to generate valves with variable macro-scale morphology and size (Fig. 2). Heart sketch adapted from Ref. [72]. In addition to a linear control over the valve thickness, DCD showed relatively homogeneous fiber deposition over the valve surface. **h)** Native porcine tricuspid valve thickness distribution over the leaflet area. **i)** Engineered tricuspid valve thickness distribution over the leaflet area after 5 h and 2 min of fabrication (thickness distribution comparison for the four valves provided in Fig. 3). (For interpretation of the references to colour in this figure legend, the reader is referred to the web version of this article.)

2.4. Engineered leaflet biaxial mechanical property measurements

The capacity to de-couple and to control in-plane and out of plane mechanics was investigated by fabricating electrospun valves with three different mandrel tangential velocities ($V_1 = 0.3$, $V_2 = 1.5$, $V_3 = 3$ m/s) and three different rastering velocities ($R_0 = 0$, $R_1 = 0.16$, $R_2 = 2.5$ cm/s). The underlying hypothesis was that while mandrel tangential velocity dictates in-plane properties such as the mechanical anisotropy [42] without affecting bending rigidity, the rastering velocity dictates the bending rigidity [34,35] without affecting the in-plane mechanics. The latter was characterized by biaxial mechanical testing [43]. Samples of 10 × 10 mm were harvested from the leaflet belly region, four polypropylene (Ethicon, Somerville, NJ) markers were placed on the corners of a squared area at the center of the sample and used to measure the deformation gradient tensor. Tests were performed using a Lagrangian

equi-stress control protocol and a maximum load of 400 kPa was adopted to induce physiologically relevant strain levels [44]. Samples ($n=3$/group) were preconditioned and then tested for 10 cycles of 15 s in PBS at room temperature. Data processing was performed with a custom-made software developed in Matlab using the free-float position of the markers following preconditioning as a reference. For each of the nine electrospun valve groups fabricated combining the three tangential V_1, V_2, V_3 and the three rastering velocities R_0, R_1, R_2 (Fig. 4a), mechanical anisotropy was quantified using the anisotropy ratio AR [42] defined as:

$$AR = \frac{(\lambda_{XD} - 1)}{(\lambda_{PD} - 1)} \tag{1}$$

where λ_{XD} and λ_{PD} represents the stretches over the cross-preferential (radial direction of the mandrel) and preferential
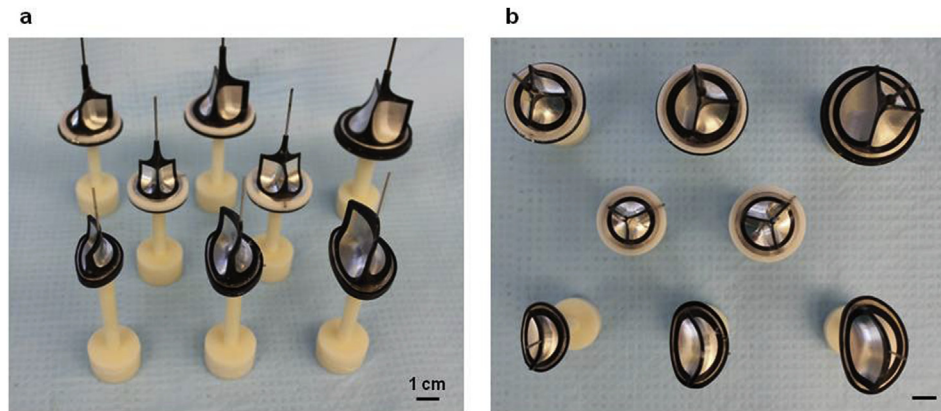
Fig. 2. DCD process control on engineered heart valve size. a) DCD mandrels side view showing top row with tricuspid valve mandrels of different sizes (diameters 26, 30 and 34 mm), middle row with pulmonary and aortic valve mandrels (diameters 20 and 23 mm), and bottom row with mitral valve mandrels (diameters 24, 30 and 34 mm). **b)** Top view of DCD mandrels showing the conductive component embedded in the non conductive framework.
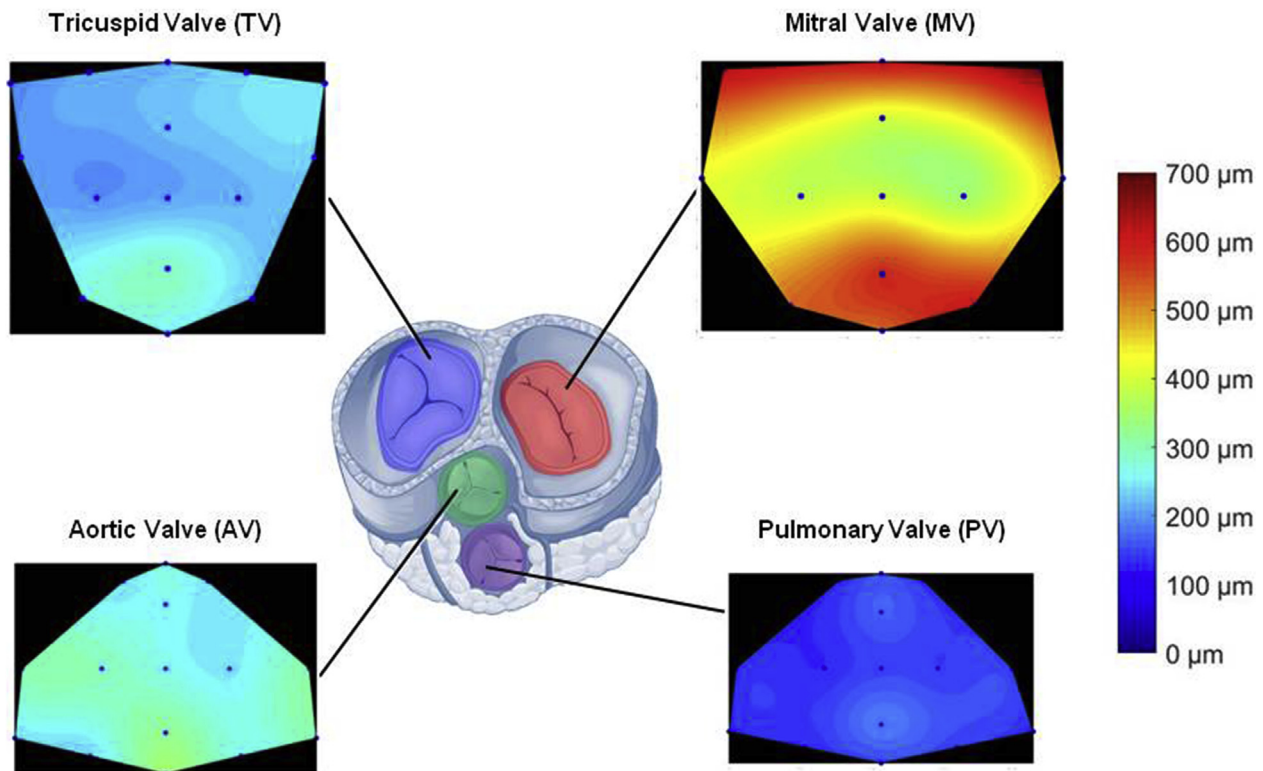

Fig. 3. Native porcine valve thickness distribution over the leaflet area for tricuspid, mitral, aortic and pulmonary valves. Consistent with the related pressure regimens LV valves showed higher thickness values when compared to the right ventricular valves. Similarly, the four valves were all thicker in the leaflet coaptation/free edge zone.

directions (circumferential direction of the mandrel) calculated at 200 kPa, respectively. In order to assess the capacity to control anisotropy, the anisotropy ratios of the nine electrospun valves groups were plotted vs. the mandrel velocities and linearly interpolated. Native porcine valve leaflets ($n=9$) were assessed with the identical biaxial testing protocol (Fig. 5). Similar to the process illustrated for the identification of the deposition time, their AR was utilized to identify the mandrel tangential velocity necessary to reproduce the same level of anisotropy of native tissue (Fig. 4b). Engineered valve leaflets fabricated with these conditions were further tested ($n = 4$) to assess the capacity of the design paradigm to control in-plane mechanics.

2.5. Engineered leaflet bending rigidity measurements

The second step in verifying DCD capacity to de-couple and to control in-plane and out of plane mechanics was assessing the leaflets bending rigidity. The nine electrospun valve groups, fabricated combining the three tangential velocities V_1, V_2, V_3 and the three rastering velocities R_0, R_1, R_2, were tested ($n = 3$/group) with a three point bending apparatus [45] and an experimental protocol [34] specifically developed for heart valve leaflets [46]. In brief, $(12-25) \times 2.5$ mm sections oriented along the radial direction of the leaflets were dissected from the belly region. Polypropylene markers were affixed along the edge of each sample 1 mm apart
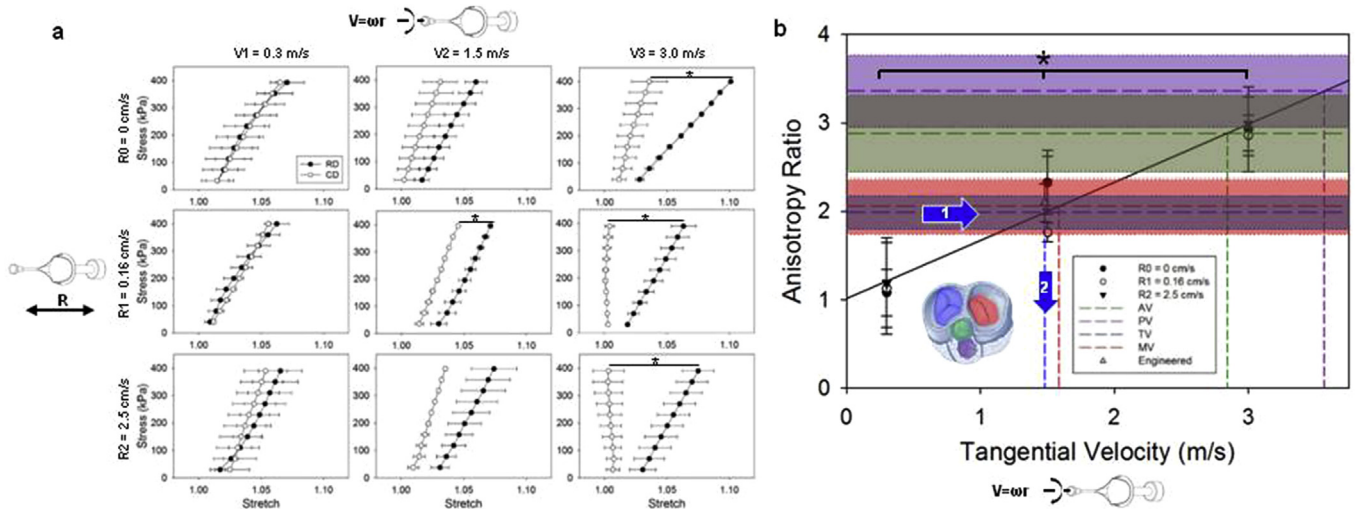
Fig. 4. DCD process control of engineered valve in-plane mechanics. a) Engineered valve in-plane mechanical response was tested with biaxial tensile testing in equi-stress mode for 9 processing conditions (data presented as mean ± sem). Altered parameters were: mandrel tangential velocity (ω(radius)), which dictates fiber alignment and as a consequence mechanical anisotropy) and rastering velocity (R, which dictates fiber intersections per area and the bending modulus). In order to demonstrate control over valve leaflet in plane and out of plane mechanics, the mandrel design was tested on 9 different configurations covering the operational range of interest for the valve application (mandrel tangential velocity: 0.3–3 [m/s], rastering linear velocity: 0–2.5 [cm/s]). The mandrel velocity affected the mechanical anisotropy (increasing difference in compliance over the mandrel radial direction for V1 = 0.3, V2 = 1.5, V3 = 3 [m/s]). In contrast, the rastering velocity did not affect the level of anisotropy. **b)** The anisotropy ratio (AR, defined as the mechanical strain ratio between the radial and circumferential directions) versus rotational velocity, for the nine fabrication conditions studied (R0, R1, R2 combined with V1, V2 and V3), was derived from the biaxial data of Fig. 2a. Native porcine valve ARs, illustrated with different colors, were determined with biaxial mechanical testing (Fig. 5). Based on a linear interpolation of the fabricated valve AR data at 0.3, 1.5, 3 [m/s], the prescribed mandrel tangential velocity to fabricate a tricuspid valve with native mechanics (1.48 m/s) was identified and a new set of valves were fabricated and characterized (engineered TV). The AR of the fabricated valves fully covers the range of interest for porcine native valves. Tangential velocities to achieve a desired AR are highlighted in color. (For interpretation of the references to colour in this figure legend, the reader is referred to the web version of this article.)
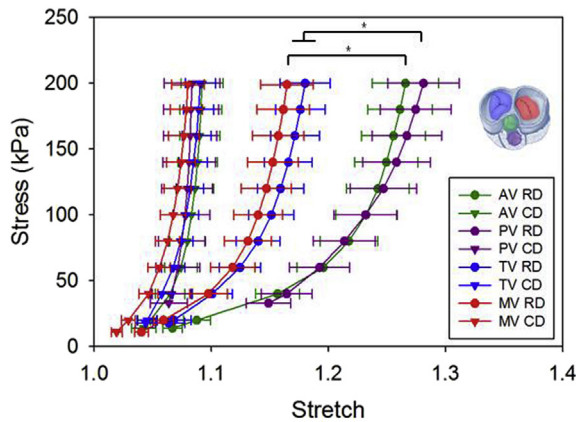

Fig. 5. Native porcine valve biaxial response for tricuspid, mitral, aortic and pulmonary valves. Consistent with the valve coaptation mechanism, based on the chordae tendineae action, atrioventricular valves (mitral and tricuspid) showed a stiffer and less anisotropic behavior when compared to the aortic and pulmonary valves.
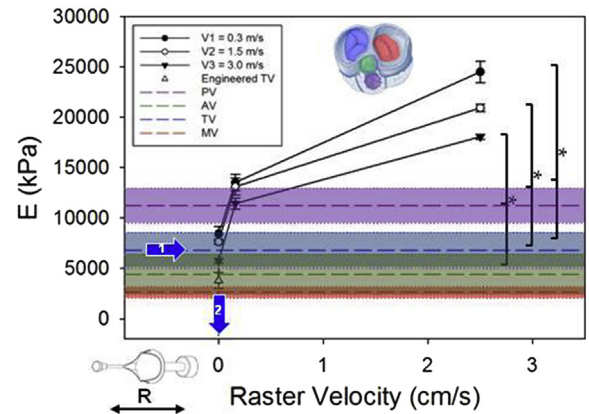

Fig. 6. DCD process control of engineered valve bending mechanics. Valve leaflet bending modulus was calculated for different values of mandrel tangential velocities (0.3, 1.5, 3 [m/s]) and rastering velocities (0, 0.16, 2.5 [cm/s]) n = 3, mean ± sem. The rastering velocity dictated the bending rigidity over a range that included the rigidity measured in atrioventricular and outflow track valve leaflets (n ≥ 7 mean ± sem). The prescribed raster velocity (0 cm/s) to achieve physiologic bending rigidity resulted in an engineered valve with rigidity below the native tricuspid valve tissue, although due to the shape of the rigidity vs. raster velocity curve in this area there is the potential for large changes in rigidity with small changes in raster velocity. Native valve leaflet thickness, elastic modulus (with AV and MV elastic moduli significantly < PV) and resulting global bending rigidity are reported in Fig. 7.

from each other, marker positions were acquired with a camera and analyzed in real-time with a custom-made program developed in LabVIEW 2010 (National Instruments, Austin, TX). Samples were placed in a custom-made holder, submerged in a PBS bath at room temperature, and connected to a vertical loading bar of known stiffness. A motorized stage (Zaber Tech, Vancouver, Canada) lowered/raised the sample against the loading bar reaching a maximum sample curvature of $\Delta k_{max} = 0.12$ mm^{-1} [34,35]. The bending modulus, E, and the bending rigidity, EI, were then calculated from the Bernoulli-Euler equation:

$$M = EI\Delta k \qquad (2)$$

where the bending moment M, the second moment of inertia I, and

the change in curvature Δk were calculated based on measured load acting on the bar, the geometry and the sample deformed configuration as described in Ref. [45]. Elastic moduli calculated for the nine experimental groups were plotted vs. the rastering velocity; native valve leaflets (n≥7) were also tested. The rastering velocity range of interest to recapitulate native bending rigidity (Figs. 6–7) was identified as described in sections 2.3–2.4 for the leaflet thickness and anisotropy ratio respectively. Based on this
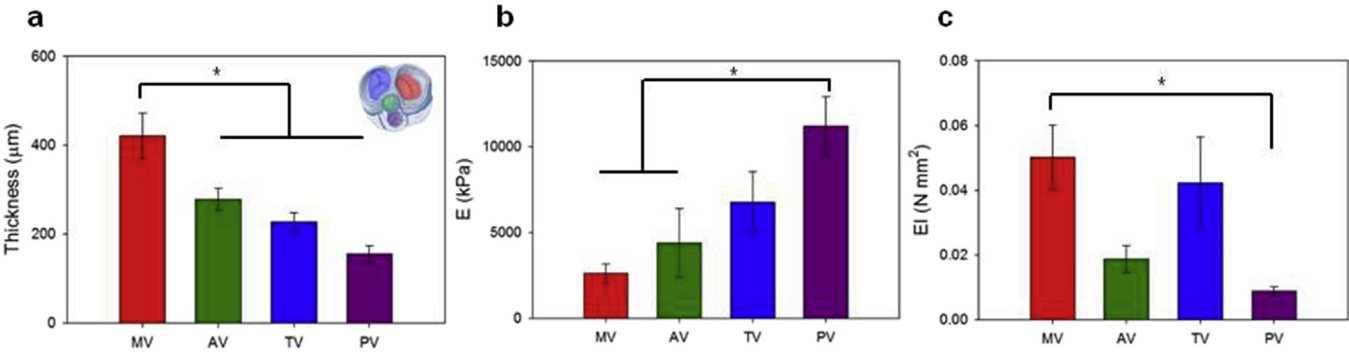
Fig. 7. Native porcine valve bending mechanics for tricuspid, mitral, aortic and pulmonary valves. a) Valve thickness (Fig. 1f) and b) bending elastic moduli (Fig. 6). c) Consistent with the biaxial response illustrated in Fig. 5 atrioventricular valves (mitral and tricuspid) showed a higher bending rigidity (EI) when compared to the outflow track (aortic and pulmonary) valves. This result was also in agreement with the valve fiber bundle diameter quantification presented in Fig. 8.
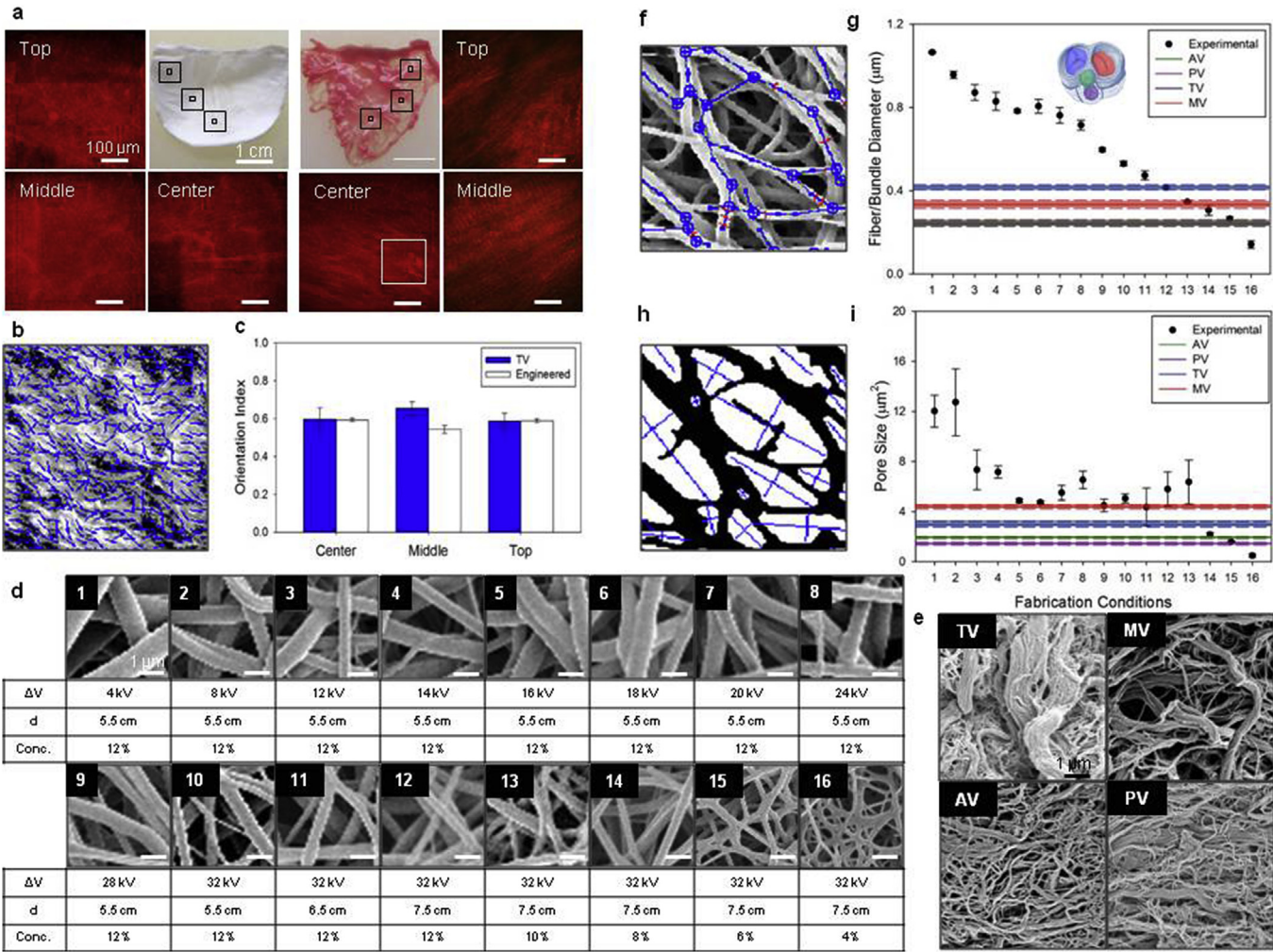

Fig. 8. DCD process control on engineered valve microstructure. a) Engineered valve leaflet fiber alignment over 3D was studied by multi-photon microscopy. Image stacks of 500 × 500 × 100 μm were analyzed at five different locations within the valve leaflet: top left and top right, center and a middle transition zone between the two (mid-leaflet left and mid-leaflet right). For comparison the same imaging and digital analysis technique was applied to native porcine TV leaflets. **b)** Detail (inset from figure **a)**, of fiber orientation detection algorithm applied to collagen fibers second harmonic generation. **c)** The level of fiber alignment in terms of the orientation index (OI) was quantified for both valve types and the top and mid-leaflet data combined (Supplemental Fig. 1). Native vs. engineered valve fiber OI comparison showed levels of fiber alignment (OI = 0.57–0.62) in engineered valve leaflets not statistically different from the native valve. Valve leaflets detailed 2D micro-architecture (Supplemental Figs. 2–4) was characterized by scanning electron microscopy **d-e)** and image analysis identifying fiber network **f)** and pores geometry **h)**. Fiber diameter and pore size for valve scaffolds fabricated at different processing conditions are provided in figure **g)** and **i)** respectively (the overlapping fiber bundle diameter range for AV and PV shown as grey). Values were compared with native valve fiber bundle diameter showing the DCD capacity to recapitulate native tissue micro-architecture.
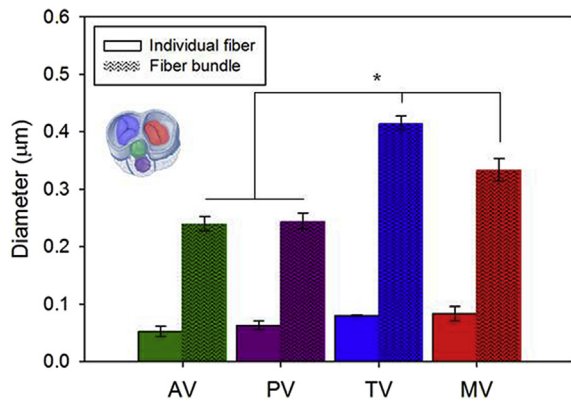
Fig. 9. **Individual fiber and fiber bundle diameter quantification for porcine heart valves**. While individual collagen fiber diameter for the four valve types showed comparable values (40—50 nm), the MT and TV (atrioventricular valves) had larger fiber bundle diameters than the AV and PV (outflow track valves). This result was also in agreement with the valve biaxial response and bending rigidity presented in Figs. 4—7, respectively.

corresponding to $n = 3$ on 5 different locations, Fig. 8a). An FV 1000 microscope (Olympus, Center Valley, PA) was set with excitation wavelength of 830 nm, laser transmissivity 2—3%, and sampling speed of 20 μs/pixel. Emission signals were acquired at 400 ± 50 nm for the native collagen fibers and at 595 ± 25 nm for the scaffold fibers. Each image stack covered a volume of ~508 × 508 × 100 μm with 10 μm steps along the z-axis. While collagen fiber emission was obtained via second harmonic generation, scaffold fiber signal was enhanced with CMTPX (Molecular Probes, Eugene, OR) following a protocol described in Ref. [41]. Digital image analysis was utilized (Fig. 8b—c, Supplemental Fig. 1) to quantify the level of fiber alignment and its related structural anisotropy, a custom made algorithm developed and adopted in Refs. [39,47] provided the fiber orientation index (OI), a well-known metric for alignment that reports a value of OI = 1 for purely parallel fibers and OI = 0.5 for isotropic arrangement [48].

Scanning electron microscopy was adopted to analyze DCD processed and native leaflet surface morphology ($n = 3$/group, Fig. 8d—e, Supplemental Fig. 2). Native valve leaflets were decellularized following the protocol described in Ref. [41]. Samples
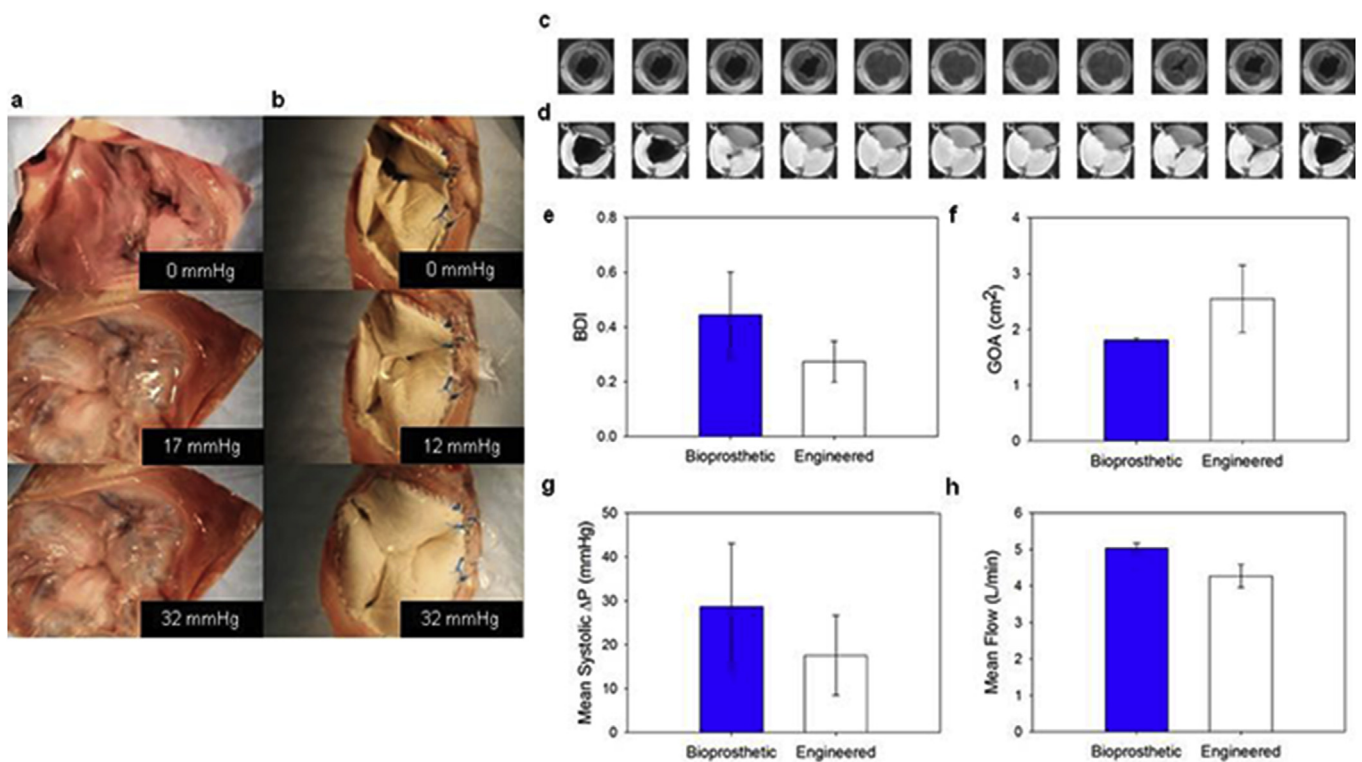

Fig. 10. **Engineered valve quasi-static behavior and valve leaflet dynamics**. Ex-vivo coaptation and valve function in pulse duplicator tests. To assess the engineered valve capacity to withstand physiologically relevant values of pressure, the prostheses were implanted *ex vivo* in the tricuspid position in porcine hearts. Healthy native porcine tricuspid valves a) were compared to the engineered valve b) showing proper leaflet coaptation at Δp> 30 mmHg and proper suture retention. c) and d) show a Carpentier-Edwards bioprosthetic and engineered valve respectively during the systolic phase (50 msec between images). e) Bending deformation index (BDI) comparison, at mid-diastole. f) Geometric orifice area comparison (GOA), at peak diastole. g) Mean systolic pressure comparison. h) Mean flow comparison. None of the comparisons presented in e-h showed statistically significant differences.

newly identified fabrication parameter, engineered valves ($n=4$) were fabricated and tested in bending.

2.6. Engineered valve leaflet fiber network micro-architecture via multi-photon imaging and scanning electron microscopy

Multi-photon imaging was utilized to study the native porcine and engineered tricuspid valve micro-architecture ($n = 15$/group

were sputter coated with Pd/Au and imaged with a standard SEM (JEOL JSM6330F). An image analysis algorithm developed in Ref. [48] was applied to the DCD leaflet samples and extracted fiber network (Fig. 8f, Supplemental Fig. 3), pores structure (Fig. 8h, Supplemental Fig. 4) and quantified a full set of micro-architecture variables (Supplemental Fig. 5) including: fiber diameter (Fig. 8g), average pore area (Fig. 8i), intersection density (number of overlaying fibers/unit area), length between fiber intersection, and pore

aspect ratio. NIH Image J was utilized for the quantification of native leaflet fiber bundle/individual fiber diameter (Figs. 8g, and 9) and average pore area (Fig. 8i).

2.7. Engineered valve quasi-static behavior: coaptation ex-vivo test

The capacity of the whole engineered valve to both retain sutures and withstand physiologically relevant values of atrio-ventricular pressure was assessed ex-vivo by filling the ventricular cavities of porcine hearts, freshly obtained from an abattoir, with PBS under quasi-static conditions (estimated leaflet strain ratio $\leq$ 10%/s). The right atrium was dissected exposing the atrio-ventricular plane, at the fibrous trigone level, to the atmospheric pressure. The native tricuspid valve was removed and replaced by the engineered valve which was implanted using a continuous polypropylene 5/0 running suture into the tricuspid annulus. The valve posts were also sutured to the papillary muscles before the running suture in order to stabilize the valve [26]. The ventricular pressure was measured with a flexible catheter (AD Instruments, Dunedin, New Zealand) equipped with a Mikro-Cath™ (Millar Inc., Houston, TX) which accessed the ventricle by a 16 gauge needle inserted in the right ventricle in proximity to the heart apex. The pulmonary trunk was sutured proximally at the pulmonary valve and secured around a silicone tube which filled the right ventricle under pressure control, reaching peak values of ~35 mmHg. Pressure signals were recorded with a NISBC68 and a custom made script developed in LabVIEW, and simultaneous digital images of the valve were acquired with a Rebel T3 camera (Canon Inc., Melville, NY) [41]. For comparison, healthy native porcine valves were tested before being removed from the ventricle under identical conditions (Fig. 10a–b, Supplemental Video 2). PEUU leaflet suture retention was further evaluated with a Tytron TM250 uniaxial tensile device equipped with a 10 lb, Model 661.11B-02 force transducer (MTS System Corp., Minneapolis, MN). Samples 1 cm in size were obtained from the belly region of different leaflets (n = 3). The specimens were oriented so that the leaflet circumferential direction was aligned with direction of the load. A single loop of 4−0 braided polyester suture with lines positioned 2 mm from each other and a 1 mm bite connected the sample to the tensile device clamps. In order to compare test results with previously reported data [49], the suture retention strength was calculated as the force at failure divided by suture diameter [N/m]. Burst pressure for both native and engineered tricuspid valve leaflets (n = 3/group) was quantified according to ASTM F2392 - (04). In brief, each leaflet was confined in-between a two component cylindrical steel holder with a cavity of 15 mm in diameter. Lateral displacement was prevented by gasket material so that each specimen could only deform along the longitudinal direction of the internal cavity. The chamber was pressurized with PBS using a PHD 2000 Harvard apparatus (Holliston, MA.) operating at a 6000 mL/h flow rate. The pressure signal was acquired with a model 07356-61 sensor (Cole Parmer, Vernon Hills, IL). Structural failure of the leaflet was also confirmed visually.

2.8. Engineered valve dynamics: valve function on pulse duplicator test

In order to evaluate valve function under physiological flow conditions, the engineered valve dynamics (n = 5, 40 mm diameter) were tested in vitro (Fig. 10c–h, Supplemental Fig. 6) and compared with a state of the art commercial prosthetic valve (n = 3, 35 mm diameter, 45 mm diameter including the sewing ring) the Carpentier-Edwards® Duraflex™ (Carpentier-Edwards, Irvine, CA). The two valve types were tested in a custom-made flow duplicator illustrated in (Supplemental Fig. 6). Pulsatile flow across the valve was generated with a Thoratec® Paracorporeal Ventricular Assist

Device™ (PVAD) system (Thoratec, Pleasanton CA), the PVAD was set to operate by a pneumatic driver Thoratec TLC-II at constant frequency of 80 beats/min and 30% ejection time, 65 mL stroke volume. The valve holder design shown in Supplemental Fig. 6b duplicated the same boundary conditions implemented for the ex-vivo coaptation test with the valve posts being sutured to three equi-spaced metallic posts (Supplemental video 3). Two Canon EFS cameras equipped with 50 mm compact-macro lens 1:2.5 (Canon Inc., Melville, NY) continuously detected valve motion, while Cole-Parmer K1VAC/30PSI sealed SS compound transducers, (Cole Palmer, Vernon Hills, IL) measured pressure across the valve and PXN in-line flow sensors, size 13 (Transonic Systems Inc. Ithaca, NY) measured the flow downstream the valve holder. A USB-6009 Data Acquisition (DAQ) unit (National Instruments, Austin, TX) and a PC running custom NI LabVIEW were adopted for synchronous acquisition of hemodynamics and dual camera views (Supplemental Fig. 6a and c). Acquired signals and frames were then processed with a dedicated Matlab code (Mathworks® Inc, Natick MA) which detected systolic and diastolic phases and performed digital image analysis on the camera views. Four main metrics were selected to quantify valve function: Bending Deformation Index (BDI), Geometric Orifice Area (GOA), mean Δp, and mean flow. The BDI, a widely adopted metric for heart valve bending rigidity was calculated at mid-diastole [50]. Similarly, the GOA, a measure of the capacity of the valve to open fully, was calculated at peak diastole as defined in Ref. [51], while mean Δp and flow were calculated in systole and during the entire cycle, respectively.

2.9. Statistical analyses

Statistical analyses were performed using Sigma plot (Systat Software Inc., Chicago, IL, USA). One-way analysis of variance (ANOVA) followed by Tukey−Kramer multiple comparison testing was utilized for comparison of multiple samples. Results are presented as mean ± standard error of the mean and differences were considered to be statistically significant at $p < 0.05$.

3. Results

3.1. Engineered leaflet thickness measurements

An example of the engineered valve produced with the DCD method is shown in Fig. 1c−e, g. The leaflet thickness vs. deposition time relationship is provided in Fig. 1f. Four groups with different deposition times were measured, an R^2 of 0.99 demonstrated a linear relationship between the variables. Based on this information, leaflets were engineered to obtain a target thickness of 227 μm which corresponded to the range of interest for the porcine native tricuspid leaflets. Engineered leaflets obtained after 5 h and 2 min of fabrication were then dissected and exhibited a thickness of 228 μm, as desired (Fig. 1f, arrows 1−2). Polymer deposition spatial uniformity was further studied by a comparison between the native and electrospun leaflets fabricated for 5 h and 2 min as shown in Fig. 1h−i. Native leaflet thickness for the four valves are shown in Fig. 3.

3.2. Engineered valves with controlled macro-scale morphology

Based on the demonstrated concept of the double component mandrel, different electrode geometries have been designed. Fig. 1g (additional information provided in Supplemental Video 1) illustrates the DCD ability to fabricate whole engineered heart valves of different size and anatomy (e.g. MV, AV, TV, PV).

3.3. Engineered leaflet biaxial mechanical property measurements

Electrospun valve biaxial response for the nine fabrication conditions studied is presented in Fig. 4a. Results showed both the capacity to tailor leaflet mechanical anisotropy and to de-couple in-plane mechanics from out of plane mechanics. When the rastering velocity was kept constant at R_0, R_1, or R_2, significantly higher values of anisotropy (V_3 - R_0, V_2 - R_1, V_3 - R_1, V_3 - R_2) were achieved by increasing the mandrel tangential velocity from V_1, to V_3. In contrast, when mandrel tangential velocity was kept constant at V_1, V_2, or V_3, changes in rastering velocity did not affect the mechanical anisotropy. These findings were also confirmed by the results in Fig. 4b where the anisotropy ratio (AR) was plotted vs. the mandrel tangential velocity. Each of the three experimental points V_1, V_2, V_3 grouped together with the three different values of rastering velocities (V_i - R_0, R_1, R_2) showed significant differences in AR (Fig. 4b). However, while the AR was a linear function ($R^2 = 0.98$) of the mandrel tangential velocity, changes in R_j did not affect the AR. Native porcine tricuspid valve AR was found to be 1.98, and engineered valves were fabricated accordingly at a mandrel tangential velocity of 1.48 m/s to reproduce this value and the resulting scaffold had an AR of 2.09. Native MV, AV, TV, PV biaxial response is provided in Fig. 5.

3.4. Engineered leaflet bending rigidity measurements

Bending moduli measured for the nine groups are shown in Fig. 6, operational range was 5000—25000 kPa. Results corroborated findings in the previous section with significant variations in bending moduli of the groups being dictated by changes in the rastering velocities. Similar to the process utilized to engineer leaflet thickness and in-plane mechanics, native porcine tricuspid valve leaflets were characterized and had an elastic modulus of 6780 kPa. Based on this information a rastering speed of 0 cm/s was utilized in an effort to recapitulate native tissue bending rigidity (Fig. 6, arrows 1—2). Leaflet thicknesses, elastic moduli (E) and bending rigidities (EI) are provided in Fig. 7.

3.5. Engineered valve leaflet fiber network micro-architecture via multi-photon imaging and scanning electron microscopy

3D micro-architecture was analyzed by multi-photon microscopy. Image stacks of engineered tricuspid and native valves are provided in Fig. 8a. Qualitative observation, performed at different locations, confirmed the fibrillar nature of the electrospun leaflets. Quantitative analysis (Fig. 8b—c, Supplemental Fig. 1) of fiber angle distribution and level of alignment corroborated the results of the in-plane mechanical characterization and revealed an anisotropy of the engineered valves comparable to the native tissue leaflets (Fig. 5). DCD process control on micro-architecture was evaluated by comparing leaflets fabricated under different conditions with decellularized porcine valve leaflets (Fig. 8d—e). 2-D topology was studied with SEM and digital image processing and included fiber network and pores morphology quantification (Fig. 8f,h, Supplemental Figs. 2—5). Fiber diameter and pore size comparisons are provided in Fig. 8g,i respectively. An additional set of morphological features (e.g. fiber intersection spatial density, pore aspect ratio, and mean distance between intersections), are presented in Supplemental Fig. 5.

3.6. Engineered valve quasi-static behavior: coaptation ex-vivo test

Native tricuspid and engineered valve quasi static behavior was compared and is reported in Fig. 10a-b. Engineered valves seeking to mimic native thickness, in-plane, and out of plane mechanics,

showed the capacity to both retain sutures and to coapt properly when exposed to a physiologically relevant atrio-ventricular pressure of ~35 mmHg (Supplemental video 1). Suture retention strength of the PEUU leaflet was equal to 4900 $\pm$ 380 N/m. Burst pressure for the native and engineered tricuspid leaflet were 987 $\pm$ 41 mmHg and 228 $\pm$ 12 mmHg respectively.

3.7. Engineered valve dynamics: valve function on pulse duplicator test

Engineered tricuspid valves with thickness, planar mechanics and bending rigidity that were targeted to approximate native tissue were compared to the bioprosthetic Carpentier-Edwards® Duraflex™ valve (Supplemental video 3). Fig. 10c—d shows a representative systolic phase. Quantitative comparisons were also conducted and included: BDI, GOA, mean systolic Δp and mean flow, (Fig. 10e—h), showing comparable behavior in the two valve types.

4. Discussion

4.1. Bioinspired control of macro-scale morphology, mechanics and micro-structure

4.1.1. Engineered leaflet thickness measurements
The electrospun leaflet thickness was generally uniform. In spite of a growing number of *in vivo* studies evaluating a broad spectrum of technical approaches to tissue-engineered scaffolds for cardiac valve replacement [10,11,15—17,26—29,32,44,52—59], critical engineering design parameters to achieve effective valve function remain ill-defined. This unfortunately includes not only simple macroscopic variables such as the leaflet thickness but also 3D micro-architecture or surface topology characteristics (e.g. pore sizes, fiber diameters, fiber interconnectivity). For instance, leaflet thicknesses that have been proposed for tissue engineered heart valves include 800—1200 μm in Ref. [59], 100—250 μm in Ref. [19] and 25 μm in Ref. [24]. This variability in approaches can be attributed to the diversity in fabrication methods, materials, and importantly, to the complex interplay between scaffold degradation and endogenous tissue formation. Given the current state of the art, this work focused on covering a broad range of values (0—500 μm). This was accomplished by demonstrating a fabrication time vs. thickness linear relationship, by selecting native tissue thickness as the targeted value for the engineering of the leaflet (Fig. 1f) and by comparing this operational range with native leaflet thickness for the four valves (Fig. 3). Interestingly, measured native leaflet thickness values followed the same relationship generally known to clinicians for physiological transvalvular pressure values with mitral (MV) > aortic (AV) > tricuspid (TV) > pulmonary (PV).

4.1.2. Engineered valves with controlled macro-scale morphology
Similar to rapid prototyping methods, the DCD approach (Fig. 1g) allows for the rapid creation (<3 h) of an engineered construct, of desired shape, at the macroscopic scale (40 mm in diameter) and yet composed of smaller characteristic elements. In contrast to current rapid prototyping technologies, DCD can achieve fibers at a smaller scale, in the 0.1—10 μm range. While Figs. 1—2 proved the capacity to control 3D shape and size of the engineered construct, recapitulating the exact native heart valve shape would require a dedicated study aiming first to identify, and then to standardize the topology of the most prominent anatomical landmarks for a native valve leaflet. This complex task extends beyond the scope of this work.

4.1.3. Engineered leaflet biaxial mechanical property measurements

Several authors have discussed the importance of tissue anisotropy [60], its implications for valve mechanobiology [44] and effective coaptation [61]. The results here provided evidence of DCD capacity to (I) fine-tune the level of anisotropy (Eq. (1)) within a range of interest (AR = 1–3.5 covering tricuspid, mitral, aortic and pulmonary valve values, Fig. 5) for the valve application (AR>1.3 [42]) and (II) de-couple the influence on in-plane from out of plane mechanics Fig. 4a–b. Similar to the leaflet thickness measurement, native valve mechanics reflected the different functions covered by the four valves. For example, anisotropy ratios measured for the AV and PV were higher than those reported for the MV and TV. The coaptation mechanism of the atrioventricular valves (MT and TV) relies not only on leaflet tissue mechanics, but also on the presence of dedicated structures, chordae tendineae, that prevent valve regurgitation. In contrast, outflow track valve (AV and PV) anatomy does not include chordae, and the capacity of the valves to prevent backflow and regurgitation is then based on the sinus of valsalva/ pulmonary sinus shape and on higher leaflet tissue anisotropy (e.g. the radial direction being more compliant, and thus capable of undergoing larger deformations and facilitating contact between a larger portion of the leaflet free edges, Fig. 5)

4.1.4. Engineered leaflet bending rigidity measurements

Engineered valves produced with these fabrication conditions exhibited an elastic modulus of 3250 kPa. Similar to the biaxial properties, the bending rigidity is another critical factor for heart valve biomechanics [44,46], which for a given geometry can only be modulated by changing the elastic bending modulus (Eq. (2)). While based on sandwich theory, this can be achieved by combining different material layers [22,34,62], and results (Fig. 6) showed the capacity to extensively modify the elastic bending modulus (E = 5000–25000 kPa) by changing the rastering speed. Thus, without altering material chemistry or composition, the same biomaterial can be adopted to reproduce different bending moduli characteristic of the different valves, a result with fundamental implications for engineered leaflets [34,35]. While native valve leaflet elastic moduli were inversely proportional to the leaflet thickness (Fig. 7), the correspondent bending rigidity (EI) was consistent with the biaxial response illustrated in Fig. 5 showing atrioventricular valves with higher bending rigidity values than those measured for the outflow track valves.

4.1.5. Engineered valve leaflet fiber network micro-architecture via multi-photon imaging and scanning electron microscopy

The relationship between leaflet structure and function was confirmed when the microstructure quantification corroborated the in-plane mechanics results (e.g. engineered leaflet AR = 2.09, Fig. 4), and scaffold fibers exhibited a level of alignment (OI = 0.57–0.62) comparable to those obtained for the collagen fibers in porcine native tricuspid valve (Fig. 8b–c). This feature will not only determine the stress distribution over the leaflet but may greatly influence subsequent cell behavior including ECM elaboration [63,64]. Consistent with differences in the role and mechanics (Figs. 5 and 7) reported between the atrioventricular and the outflow track valves, MT and TV had larger fiber bundle diameters when compared to the AV and PV (Fig. 9). It can be speculated that this difference in size is due to the presence of the chordae tendineae in MT and TV. These macro-scale leaflet structural elements are hierarchically composed by fiber bundles which in turn are made at the microscopic level of single collagen fibers. One might expect that a larger structural element at the macro-scale (chordae tendineae) would be coupled with a larger diameter on the hierarchically connected structural elements at smaller scales (bundles and individual collagen fibers). The results support

this expectation when the valve ultrastructure is analyzed. Also shown is the capacity of the DCD process to fully cover the fiber bundle diameter and pore size ranges measured for the native heart valves (Fig. 8g,i).

4.1.6. Engineered valve quasi-static behavior: coaptation ex-vivo test

Suture retention as well as the capacity to withstand a pressure of 32 mmHg, physiologically relevant for the tricuspid indication (>25 mmHg [60]), was evaluated, reproducing ex vivo the closest anatomical [26] and mechanical conditions to the in vivo scenario (Fig. 10a–b, Supplemental video 1). Burst pressure of the native tissue was significantly higher than that measured for the engineered valve. The pressure vs. time signal during the burst test was consistent with this finding, showing a sharper profile for the native tissue samples. This latter observation might be explained by the presence of a continuous layer of endothelial cells that diminishes the permeability to fluids of the native tissue. The suture retention strength measured for the engineered leaflet was comparable (11200 N/m [49]) to previously reported data.

4.1.7. Engineered valve dynamics: valve function on pulse duplicator test

The DCD engineered valve showed equivalent performance when compared on a pulse duplicator to the Carpentier-Edwards® Duraflex™ valve. This assessment included qualitative (Fig. 10 c–d, Supplemental video 2) observation as well as quantitative metrics (Fig. 10 c–d, Supplemental Fig. 6). Consistent with Erasmi et al. [50] who reported values of 0.15–0.8, the BDI range was 0.2–0.5. Similarly, the GOA was 1.5–3 cm^2, values within the same range calculated in Ref. [51] for a number of commercial devices (e.g. Trifecta™, Magna Ease™, Mitro Flow™, Soprano Armonia™).

4.2. Tissue engineered heart valves: a brief technology overview from a structure - function perspective

Shinoka et al. [10,57] pioneered the notion of engineered tissue leaflets utilizing non-woven biodegradable scaffolds, with later studies adding new levels of complexity by assembling composite meshes [12]. In spite of this versatility, non-woven meshes or composites do not allow for full control of the fiber network orientation, leaflet anisotropy and bending rigidity. As an alternative to the regeneration approach described, the repopulation model [7,8] employs a previously decellularized allograft [27,28] or xenograft [30,55,65] that is repopulated with cells and finally implanted. In order to combine the advantages of native tissue derived valves such as progressive endothelialization in vivo and constructive tissue remodeling with the capacity to engineer construct mechanics, Seydan et al. introduced [33] and later refined [59] an innovative notion of cultured cell-derived matrix. However, mechanical properties largely depend on the modality and efficacy of the conditioning regimen adopted. Kluin et al. [66]. combined a polyether etherketone reinforcement ring with an electrospun conduit demonstrating sustained valve function and in situ tissue growth on a sheep model up to 12 months in the pulmonary position. The Grande-Allen group has investigated the possibility of combining electrospun meshes with desired mechanics and cell-seeded hydrogels [22,62] with bioactivity. Nevertheless, the majority of these techniques were applied to leaflet processing or relied on a stent to sustain physiologically relevant function and as such, were not able to guaranty both control on the mechanics and produce fully assembled, stent-less, valve constructs. The Parker group has pioneered rotary jet spinning of polymer - gel nanofibers [67], and most recently this technique has been refined and combined with custom sized mandrels [68]. However, construct

mechanics and properties were dependent on the polymer-gel ratios. The DCD processing method enhanced the capacity to control in-plane (Fig. 4) and out of plane mechanics (Fig. 6), and also showed the unique ability to modulate these features while controlling leaflet microstructure (Fig. 8) and depositing micro-fibers on macro-scale, morphology-inspired fully assembled valves (Fig. 1).

4.3. DCD valve limitations and future work

In spite of the competitive advantages illustrated, technical as well as conceptual challenges still exist. Control over bending rigidity remains limited due to the non-linearity of the rastering speed versus elastic modulus relationship at low rastering speeds (Fig. 6), also previously reported in Refs. [34,35]. The native leaflet physiological range of interest for bending rigidity was concentrated within this non-linear characteristic region for PEUU with values for the MV falling outside the operational range. Therefore, capturing MV response in bending as well as increasing the level of control over bending rigidity is possible, but would require the adoption of a different polymer with a lower elastic modulus than PEUU. At the same time, the use of three point bending tests on valve leaflets to evaluate elastic moduli is affected by a number of experimental sources of error including: effects of testing curvature, image processing routine interpolation of bent configurations, and sample thickness measurements. Yet, controlling and characterizing native [46] or engineered leaflet [34] bending rigidity remains a crucial and perhaps underestimated endpoint in artificial valve technology [60,69]. This emphasizes the need for more accurate and commercially available testing devices to assess small biological samples (~20 mm length x 2 mm width x 0.2 mm thickness).

Non-linearity of the native leaflet biaxial response is a combined effect of the progressive recruitment of the micro-fiber network and of the intrinsic mechanical properties of the tissue [70]. DCD is a processing method capable of controlling fiber alignment. However, while this induces different fiber recruitment mechanisms and indirectly affects the non-linearity, it does not allow the full recapitulation of the native tissue constitutive response. Furthermore, control over anisotropy (Fig. 4) is dictated by the capacity to control microstructure and induce fiber alignment; this in turn depends on the mandrel tangential speed, which is a linear function of the valve radius. Therefore, smaller devices, needed for aortic and pulmonary indications, will require higher rotational speeds. This, in conjunction with mandrel concavity, conflicts with the need for accurate and controllable fiber deposition. In order to minimize these issues a second generation of DCD mandrels has been designed with nested metallic components inside the non-conductive shield (Figs. 1g and 5) as opposed to the two part design shown in Fig. 1a where the conductive component rests on the insulating one. However, with only exception of the control on shape illustrated in Fig. 1g, the current report does not include data characterizing the second generation of DCD mandrels. Single shaft mandrel geometry, robotic control of nozzle kinematics, and surface treatment to enhance/inhibit electrical conductivity are among the future design refinements that may increase the quality of the fiber deposition.

While the pulse duplicator experiments allowed for quantitative and robust comparison of valve dynamic performance (Fig. 10c–h), the valve holder did not recapitulate right heart shape and mechanical compliance (Supplemental Fig. 6). Similarly, the ex-vivo test assessed valve suture retention properties and leaflet coaptation under quasi-static conditions (Fig. 10a–b). Only large animal in-vivo assessment of this technology will provide refined assessment of engineered valve passive and dynamic function. Ultimately, while this report provides extensive in vitro characterization of the

DCD technology, and while the notion of bioinspired control of structure and function is recognized as a promising strategy to enhanced TEHV performance, the approach remains unexplored in vivo. This gap in knowledge includes the effects of native mechanics and anatomy-inspired macroscopic geometries, as well as micro-structural features such as fiber diameter and pore size. For example, reproducing native tissue-like fiber and fiber bundle diameter (<0.5 μm) might compromise cell penetration into the scaffold.

The general question remains open as to what extent an engineered valve should mimic native tissue structure, function and functional heterogeneity [7,8]. Furthermore, it seems reasonable that scaffolds of the future will be designed to meet definitive structural and functional endpoints [69,71]. However, as tissue remodeling and growth occur after implantation, the implanted valve may stray from the original design endpoints and do so in a variable manner. Finally, while this complexity currently represents a limiting factor for medical devices based on the notion of endogenous tissue growth, the processing technology discussed herein is also applicable to permanent, non degradable biomaterials.

5. Conclusion

Fibrillar structures are ubiquitous in biology, their advantages for the effective engineering of heart valve tissue and their potential as viable scaffolds for the endogenous tissue growth paradigm are widely accepted. Within this category, spun meshes and fiber reinforced composites provide a number of incremental benefits when compared with non-woven, amorphous, native tissue or ECM-derived scaffolds. These include more accurate and tunable control of construct macro- and micro-architecture as well as more robust control over the biaxial mechanical response. Results in this report proved that the DCD technique maintains these benefits, but also extends them further by allowing for the fabrication of fully assembled stent-less multi-leaflet valves, and most importantly, by possessing the ability to engineer all of these features to achieve adequate organ level mechanical function. Using the DCD method, the proper integration of these four design factors: I) macroscopic shape and size, II) in-plane mechanics, III) out of plane mechanics, IV) microstructure, within one material processing platform may lead to structure-function enhanced generation of engineered valves. More broadly, this study introduces and characterizes electrodes for electrospinning based on the concept of multiple components made of electrically conducting/insulating materials to selectively orient fiber deposition in the context of a complex macro-scale morphology. Although the data presented are strictly related to the heart valve application, DCD potentially extends beyond with electrode geometries, materials and kinematics that can be designed to engineer scaffolds for a larger variety of applications or tissue types such as bladder, trachea, branched vascular grafts and meniscus. Cumulatively these findings and concepts offer DCD as a promising and versatile processing methodology with a distinctive capacity to control structure and function.

Appendix A. Supplementary data

Supplementary data related to this article can be found at https://doi.org/10.1016/j.biomaterials.2017.10.011.

References

[1] V.T. Nkomo, J.M. Gardin, T.N. Skelton, J.S. Gottdiener, C.G. Scott, M. Enriquez-Sarano, Burden of valvular heart diseases: a population-based study, Lancet 368(9540) 1005-1011.

[2] B. Iung, A. Vahanian, Epidemiology of valvular heart disease in the adult, Nat. Rev. Cardiol. 8 (3) (2011) 162–172.

[3] B. Iung, G. Baron, E.G. Butchart, F. Delahaye, C. Gohlke-Bärwolf, O.W. Levang, P. Tornos, J.-L. Vanoverschelde, F. Vermeer, E. Boersma, P. Ravaud, A. Vahanian, A prospective survey of patients with valvular heart disease in europe: the euro heart survey on valvular heart disease, Eur. heart J. 24 (13) (2003) 1231–1243.

[4] Edwards Lifesciences 2015 year report.

[5] K. Hammermeister, G.K. Sethi, W.G. Henderson, F.L. Grover, C. Oprian, S.H. Rahimtoola, Outcomes 15 years after valve replacement with a mechanical versus a bioprosthetic valve: final report of the Veterans Affairs randomized trial, J. Am. Coll. Cardiol. 36 (4) (2000) 1152–1158.

[6] M. Arsalan, T. Walther, Durability of prostheses for transcatheter aortic valve implantation, Nat. Rev. Cardiol. 13 (6) (2016) 360–367.

[7] I. Vesely, Heart valve tissue engineering, Circ. Res. 97 (8) (2005) 743–755.

[8] M.H. Yacoub, J.J.M. Takkenberg, Will heart valve tissue engineering change the world? Nat. Clin. Pract. Cardiovasc Med. 2 (2) (2005) 60–61.

[9] M.Y. Emmert, E.S. Fioretta, S.P. Hoerstrup, Translational challenges in cardiovascular tissue engineering, J. Cardiovasc. Transl. Res. (2017) 1–11.

[10] T. Shinoka, D. Shum-Tim, P.X. Ma, R.E. Tanel, R. Langer, J.P. Vacanti, J.E. Mayer Jr., Tissue-engineered heart valve leaflets: does cell origin affect outcome? Circulation 96 (9 Suppl) (1997) 102–107. II.

[11] R. Sodian, S.P. Hoerstrup, J.S. Sperling, S. Daebritz, D.P. Martin, A.M. Moran, B.S. Kim, F.J. Schoen, J.P. Vacanti, J.E. Mayer, Early in vivo experience with tissue-engineered trileaflet heart valves, Circulation 102 (suppl 3) (2000). Iii-22-Iii-29.

[12] G. Zund, C. Breuer, T. Shinoka, P. Ma, R. Langer, J. Mayer, J. Vacanti, The in vitro construction of a tissue engineered bioprosthetic heart valve, Eur. J. Cardio Thoracic Surg. 11 (3) (1997) 493–497.

[13] A. Mol, N.J. Driessen, M.C. Rutten, S.P. Hoerstrup, C.V. Bouten, F.P. Baaijens, Tissue engineering of human heart valve leaflets: a novel bioreactor for a strain-based conditioning approach, Ann. Biomed. Eng. 33 (12) (2005) 1778–1788.

[14] J.M. Reimer, Z.H. Syedain, B.H. Haynie, R.T. Tranquillo, Pediatric tubular pulmonary heart valve from decellularized engineered tissue tubes, Biomaterials (2015).

[15] M.Y. Emmert, B. Weber, L. Behr, S. Sammut, T. Frauenfelder, P. Wolint, J. Scherman, D. Bettex, J. Grünenfelder, V. Falk, Transcatheter aortic valve implantation using anatomically oriented, marrow stromal cell-based, stented, tissue-engineered heart valves: technical considerations and implications for translational cell-based heart valve concepts, Eur. J. Cardio Thoracic Surg. 45 (1) (2014) 61–68.

[16] H. Spriestersbach, A. Prudlo, M. Bartosch, B. Sanders, T. Radtke, F.P. Baaijens, S.P. Hoerstrup, F. Berger, B. Schmitt, First percutaneous implantation of a completely tissue-engineered self-expanding pulmonary heart valve prosthesis using a newly developed delivery system: a feasibility study in sheep, Cardiovasc. Interv. Ther. (2016) 1–12.

[17] S.P. Hoerstrup, R. Sodian, S. Daebritz, J. Wang, E.A. Bacha, D.P. Martin, A.M. Moran, K.J. Guleserian, J.S. Sperling, S. Kaushal, Functional living trileaflet heart valves grown in vitro, Circulation 102 (suppl 3) (2000). Iii-44-Iii-49.

[18] R. Sodian, M. Loebe, A. Hein, D.P. Martin, S.P. Hoerstrup, E.V. Potapov, H. Hausmann, T. Lueth, R. Hetzer, Application of stereolithography for scaffold fabrication for tissue engineered heart valves, Asaio J. 48 (1) (2002) 12–16.

[19] A.G. Kidane, G. Burriesci, M. Edirisinghe, H. Ghanbari, P. Bonhoeffer, A.M. Seifalian, A novel nanocomposite polymer for development of synthetic heart valve leaflets, Acta Biomater. 5 (7) (2009) 2409–2417.

[20] B. Rahmani, S. Tzamtzis, H. Ghanbari, G. Burriesci, A.M. Seifalian, Manufacturing and hydrodynamic assessment of a novel aortic valve made of a new nanocomposite polymer, J. Biomechanics 45 (7) (2012) 1205–1211.

[21] M. Weber, E. Heta, R. Moreira, V.N. Gesche, T. Schermer, J. Frese, S. Jockenhoevel, P. Mela, Tissue-engineered fibrin-based heart valve with a tubular leaflet design, Tissue Eng. Part C. Methods 20 (4) (2013) 265–275.

[22] H. Tseng, D.S. Puperi, E.J. Kim, S. Ayoub, J.V. Shah, M.L. Cuchiara, J.L. West, K.J. Grande-Allen, Anisotropic poly(ethylene glycol)/polycaprolactone hydrogel–fiber composites for heart valve tissue engineering, Tissue Eng. Part A 20 (19–20) (2014) 2634–2645.

[23] J. Sohier, I. Carubelli, P. Sarathchandra, N. Latif, A.H. Chester, M.H. Yacoub, The potential of anisotropic matrices as substrate for heart valve engineering, Biomaterials 35 (6) (2014) 1833–1844.

[24] S.H. Alavi, A. Kheradvar, A hybrid tissue-engineered heart valve, Ann. Thorac. Surg. 99 (6) (2015) 2183–2187.

[25] S.H. Alavi, W.F. Liu, A. Kheradvar, Inflammatory response assessment of a hybrid tissue-engineered heart valve leaflet, Ann. Biomed. Eng. 41 (2) (2013) 316–326.

[26] A.M. Fallon, T.T. Goodchild, J.L. Cox, R.G. Matheny, In vivo remodeling potential of a novel bioprosthetic tricuspid valve in an ovine model, J. Thorac. Cardiovasc. Surg. 148 (1) (2014) 333–340 e1.

[27] P.M. Dohmen, S. Hauptmann, A. Terytze, W.F. Konertz, In-vivo repopularization of a tissue-engineered heart valve in a human subject, J. Heart Valve Dis. 16 (4) (2007) 447.

[28] P.M. Dohmen, A. Lembcke, H. Hotz, D. Kivelitz, W.F. Konertz, Ross operation with a tissue-engineered heart valve, Ann. Thorac. Surg. 74 (5) (2002) 1438–1442.

[29] G. Perri, A. Polito, C. Esposito, S.B. Albanese, P. Francalanci, G. Pongiglione, A. Carotti, Early and late failure of tissue-engineered pulmonary valve conduits used for right ventricular outflow tract reconstruction in patients with congenital heart disease, Eur. J. Cardio Thoracic Surg. (2012), ezr221.

[30] P. Simon, M. Kasimir, G. Seebacher, G. Weigel, R. Ullrich, U. Salzer-Muhar, E. Rieder, E. Wolner, Early failure of the tissue engineered porcine heart valve SYNERGRAFT® in pediatric patients, Eur. J. Cardio Thoracic Surg. 23 (6) (2003) 1002–1006.

[31] M.E. Tedder, J. Liao, B. Weed, C. Stabler, H. Zhang, A. Simionescu, D.T. Simionescu, Stabilized collagen scaffolds for heart valve tissue engineering, Tissue Eng. Part A 15 (6) (2008) 1257–1268.

[32] K. Hayashida, K. Kanda, H. Yaku, J. Ando, Y. Nakayama, Development of an in vivo tissue-engineered, autologous heart valve (the biovalve): preparation of a prototype model, J. Thorac. Cardiovasc. Surg. 134 (1) (2007) 152–159.

[33] Z.H. Syedain, M.T. Lahti, S.L. Johnson, P.S. Robinson, G.R. Ruth, R.W. Bianco, R.T. Tranquillo, Implantation of a tissue-engineered heart valve from human fibroblasts exhibiting short term function in the sheep pulmonary artery, Cardiovasc. Eng. Technol. 2 (2) (2011) 101–112.

[34] N.J. Amoroso, A. D'Amore, Y. Hong, C.P. Rivera, M.S. Sacks, W.R. Wagner, Microstructural manipulation of electrospun scaffolds for specific bending stiffness for heart valve tissue engineering, Acta Biomater. 8 (12) (2012) 4268–4277.

[35] N.J. Amoroso, A. D'Amore, Y. Hong, W.R. Wagner, M.S. Sacks, Elastomeric electrospun polyurethane scaffolds: the interrelationship between fabrication conditions, fiber topology, and mechanical properties, Adv. Mater. 23 (1) (2011) 106–111.

[36] L. Ring, B.S. Rana, A. Kydd, J. Boyd, K. Parker, R.A. Rusk, Dynamics of the tricuspid valve annulus in normal and dilated right hearts: a three-dimensional transoesophageal echocardiography study, Eur. Heart J. - Cardiovasc. Imaging 13 (9) (2012) 756–762.

[37] H. Jiang, G. Campbell, D. Boughner, W.-K. Wan, M. Quantz, Design and manufacture of a polyvinyl alcohol (PVA) cryogel tri-leaflet heart valve prosthesis, Med. Eng. Phys. 26 (4) (2004) 269–277.

[38] J. Guan, M.S. Sacks, E.J. Beckman, W.R. Wagner, Biodegradable poly(ether ester urethane)urea elastomers based on poly(ether ester) triblock copolymers and putrescine: synthesis, characterization and cytocompatibility, Biomaterials 25 (1) (2004) 85–96.

[39] K. Takanari, Y. Hong, R. Hashizume, A. Huber, N.J. Amoroso, A. D'Amore, S.F. Badylak, W.R. Wagner, Abdominal wall reconstruction by a regionally distinct biocomposite of extracellular matrix digest and a biodegradable elastomer, J. Tissue Eng. Regen. Med. 10 (9) (2016) 748–761.

[40] A. D'Amore, J.S. Soares, J.A. Stella, W. Zhang, N.J. Amoroso, J.J.E. Mayer, W.R. Wagner, M.S. Sacks, Large strain stimulation promotes extracellular matrix production and stiffness in an elastomeric scaffold model, J. Mech. Behav. Biomed. Mater. 62 (2016) 619–635.

[41] A. D'Amore, T. Yoshizumi, S.K. Luketich, M.T. Wolf, X. Gu, M. Cammarata, R. Hoff, S.F. Badylak, W.R. Wagner, Bi-layered polyurethane – extracellular matrix cardiac patch improves ischemic ventricular wall remodeling in a rat model, Biomaterials 107 (2016) 1–14.

[42] T. Courtney, M.S. Sacks, J. Stankus, J. Guan, W.R. Wagner, Design and analysis of tissue engineering scaffolds that mimic soft tissue mechanical anisotropy, Biomaterials 27 (19) (2006) 3631–3638.

[43] M.S. Sacks, Biaxial mechanical evaluation of planar biological materials, J. Elast. Phys. Sci. solids 61 (1) (2000) 199.

[44] N.J.B. Driessen, A. Mol, C.V.C. Bouten, F.P.T. Baaijens, Modeling the mechanics of tissue-engineered human heart valve leaflets, J. Biomechanics 40 (2) (2007) 325–334.

[45] A. Mirnajafi, J. Raymer, M.J. Scott, M.S. Sacks, The effects of collagen fiber orientation on the flexural properties of pericardial heterograft biomaterials, Biomaterials 26 (7) (2005) 795–804.

[46] W. David Merryman, H.-Y. Shadow Huang, F.J. Schoen, M.S. Sacks, The effects of cellular contraction on aortic valve leaflet flexural stiffness, J. Biomechanics 39 (1) (2006) 88–96.

[47] D.M. Sánchez-Palencia, A. D'Amore, A. González-Mancera, W.R. Wagner, J.C. Briceño, Effects of fabrication on the mechanics, microstructure and micromechanical environment of small intestinal submucosa scaffolds for vascular tissue engineering, J. Biomechanics 47 (11) (2014) 2766–2773.

[48] A. D'Amore, J.A. Stella, W.R. Wagner, M.S. Sacks, Characterization of the complete fiber network topology of planar fibrous tissues and scaffolds, Biomaterials 31 (20) (2010) 5345–5354.

[49] J.J. Stankus, L. Soletti, K. Fujimoto, Y. Hong, D.A. Vorp, W.R. Wagner, Fabrication of cell microintegrated blood vessel constructs through electrohydrodynamic atomization, Biomaterials 28 (17) (2007) 2738–2746.

[50] A. Erasmi, H.-H. Sievers, T. Scharfschwerdt, T. Eckel, M. Misfeld, In vitro hydrodynamics, cusp-bending deformation, and root distensibility for different

types of aortic valve–sparing operations: remodeling, sinus prosthesis, and reimplantation, J. Thorac. Cardiovasc. Surg. 130 (4) (2005) 1044–1049.

[51] G. Tasca, R. Vismara, G.B. Fiore, A. Mangini, C. Romagnoni, A. Redaelli, C. Antona, A comprehensive fluid dynamic and geometric Study for an "In-Vitro" comparison of four surgically implanted pericardial stented valves, J. Heart Valve Dis. 24 (5) (2015) 596–603.

[52] G. De Visscher, I. Vranken, A. Lebacq, C. Van Kerrebroeck, J. Ganame, E. Verbeken, W. Flameng, In vivo cellularization of a cross-linked matrix by intraperitoneal implantation: a new tool in heart valve tissue engineering, Eur. heart J. 28 (11) (2007) 1389–1396.

[53] P.M. Dohmen, S. Ozaki, R. Nitsch, J. Yperman, W. Flameng, W. Konertz, A tissue engineered heart valve implanted in a juvenile sheep model, Med. Sci. Monit. 9 (4) (2003) BR97–BR104.

[54] D. Gottlieb, T. Kunal, S. Emani, E. Aikawa, D.W. Brown, A.J. Powell, A. Nedder, G.C. Engelmayr, J.M. Melero-Martin, M.S. Sacks, In vivo monitoring of function of autologous engineered pulmonary valve, J. Thorac. Cardiovasc. Surg. 139 (3) (2010) 723–731.

[55] A. Metzner, U.A. Stock, K. Iino, G. Fischer, T. Huemme, J. Boldt, J.H. Braesen, B. Bein, J. Renner, J. Cremer, Percutaneous pulmonary valve replacement: autologous tissue-engineered valved stents, Cardiovasc. Res. 88 (3) (2010) 453–461.

[56] D. Schmidt, P.E. Dijkman, A. Driessen-Mol, R. Stenger, C. Mariani, A. Puolakka, M. Rissanen, T. Deichmann, B. Odermatt, B. Weber, Minimally-invasive implantation of living tissue engineered heart valves: a comprehensive approach from autologous vascular cells to stem cells, J. Am. Coll. Cardiol. 56 (6) (2010) 510–520.

[57] T. Shinoka, P.X. Ma, D. Shum-Tim, C.K. Breuer, R.A. Cusick, G. Zund, R. Langer, J.P. Vacanti, J.E. Mayer Jr., Tissue-engineered heart valves. Autologous valve leaflet replacement study in a lamb model, Circulation 94 (9 Suppl) (1996) II164–II168.

[58] P. Simon, M.T. Kasimir, G. Seebacher, G. Weigel, R. Ullrich, U. Salzer-Muhar, E. Rieder, E. Wolner, Early failure of the tissue engineered porcine heart valve SYNERGRAFT® in pediatric patients, Eur. J. Cardio Thoracic Surg. 23 (6) (2003) 1002–1006.

[59] Z. Syedain, J. Reimer, J. Schmidt, M. Lahti, J. Berry, R. Bianco, R.T. Tranquillo, 6-Month aortic valve implantation of an off-the-shelf tissue-engineered valve in sheep, Biomaterials 73 (2015) 175–184.

[60] A. Hasan, K. Ragaert, W. Swieszkowski, Š. Selimović, A. Paul, G. Camci-Unal, M.R. Mofrad, A. Khademhosseini, Biomechanical properties of native and tissue engineered heart valve constructs, J. Biomechanics 47 (9) (2014) 1949–1963.

[61] S. Loerakker, G. Argento, C.W. Oomens, F.P. Baaijens, Effects of valve geometry and tissue anisotropy on the radial stretch and coaptation area of tissue-engineered heart valves, J. biomechanics 46 (11) (2013) 1792–1800.

[62] D.S. Puperi, A. Kishan, Z.E. Punske, Y. Wu, E. Cosgriff-Hernandez, J.L. West, K.J. Grande-Allen, Electrospun polyurethane and hydrogel composite scaffolds as biomechanical mimics for aortic valve tissue engineering, ACS Biomaterials Sci. Eng. 2 (9) (2016) 1546–1558.

[63] N.J. Driessen, A. Mol, C.V. Bouten, F.P. Baaijens, Modeling the mechanics of tissue-engineered human heart valve leaflets, J. biomechanics 40 (2) (2007) 325–334.

[64] J.A. Stella, J. Liao, Y. Hong, W. David Merryman, W.R. Wagner, M.S. Sacks, Tissue-to-cellular level deformation coupling in cell micro-integrated elasto-meric scaffolds, Biomaterials 29 (22) (2008) 3228–3236.

[65] G. Perri, A. Polito, C. Esposito, S.B. Albanese, P. Francalanci, G. Pongiglione, A. Carotti, Early and late failure of tissue-engineered pulmonary valve con-duits used for right ventricular outflow tract reconstruction in patients with congenital heart disease, Eur. J. Cardio Thoracic Surg. 41 (6) (2012) 1320–1325.

[66] J. Kluin, H. Talacua, A.I.P.M. Smits, M.Y. Emmert, M.C.P. Brugmans, E.S. Fioretta, P.E. Dijkman, S.H.M. Söntjens, R. Duijvelshoff, S. Dekker, M.W.J.T. Janssen-van den Broek, V. Lintas, A. Vink, S.P. Hoerstrup, H.M. Janssen, P.Y.W. Dankers, F.P.T. Baaijens, C.V.C. Bouten, In situ heart valve tissue engineering using a bioresorbable elastomeric implant – from material design to 12 months follow-up in sheep, Biomaterials 125 (2017) 101–117.

[67] M.R. Badrossamay, K. Balachandran, A.K. Capulli, H.M. Golecki, A. Agarwal, J.A. Goss, H. Kim, K. Shin, K.K. Parker, Engineering hybrid polymer-protein super-aligned nanofibers via rotary jet spinning, Biomaterials 35 (10) (2014) 3188–3197.

[68] A.K. Capulli, M.Y. Emmert, F.S. Pasqualini, D. Kehl, E. Caliskan, J.U. Lind, S.P. Sheehy, S.J. Park, S. Ahn, B. Weber, J.A. Goss, S.P. Hoerstrup, K.K. Parker, JetValve: rapid manufacturing of biohybrid scaffolds for biomimetic heart valve replacement, Biomaterials 133 (2017) 229–241.

[69] M.S. Sacks, F.J. Schoen, John E. Mayer Jr., Bioengineering challenges for heart valve tissue engineering, Annu. Rev. Biomed. Eng. 11 (1) (2009) 289–313.

[70] J.A. Stella, A. D'Amore, W.R. Wagner, M.S. Sacks, On the biomechanical func-tion of scaffolds for engineering load-bearing soft tissues, Acta Biomater. 6 (7) (2010) 2365–2381.

[71] W.D. Merryman, G.C. Engelmayr, J. Liao, M.S. Sacks, Defining biomechanical endpoints for tissue engineered heart valve leaflets from native leaflet properties, Prog. Pediatr. Cardiol. 21 (2) (2006) 153–160.

[72] J.G. Betts, P. Desaix, E.W. Johnson, J.E. Johnson, O. Korol, D. Kruse, B. Poe, J. Wise, Anatomy and Physiology, OpenStax College, 2013.